Antiferromagnetic thickness and temperature dependence of the exchange bias properties of Co/IrMn nanodots and continuous films: A Monte Carlo study

H. Kanso, Renaud Patte, Denis Ledue

24-06-2019

Antiferromagnetic thickness and temperature dependence of the exchange bias properties of Co/IrMn nanodots and continuous films: A Monte Carlo study

H. Kanso, R. Patte and D. Ledue

Normandie Université, UNIROUEN, INSA Rouen, CNRS, GPM, 76800 Saint-Etienne du Rouvray, France

Abstract

Motivated by the challenge of understanding the complex influence of the antiferromagnetic (AF) thickness and the temperature on exchange bias (EB) properties, and by the necessity of miniaturization of devices, we investigate EB properties of Co/IrMn nanodots and of continuous films by using kinetic Monte Carlo simulations. To that purpose, we use a granular model, which takes into account disordered interfacial phases in the AF layer and, in the case of nanodots, disordered phases at the edges in the AF layer. Our results show that the AF thickness dependence of the exchange field H_E (measured at room temperature) in both nanodots and continuous films exhibits a maximum in agreement with experimental results. We explain these results in terms of superparamagnetic and blocked grains in the AF layer at room temperature and also not polarized AF grains during the initial field-cooling. The simulated values of H_E in nanodots are smaller than that in continuous films for small AF thicknesses and larger for larger ones due to the contribution of the disordered phases at the edges in the AF layer. Also, we investigate the temperature and AF thickness effects on H_E and on the coercive field H_C. We found that H_E slightly decreases at low temperatures due to the disordered interfacial phases. Importantly, at the maximum blocking temperature of the AF grains, H_E vanishes and H_C exhibits a maximum. Our numerical results are successfully compared to experimental data on Co/IrMn bilayers for various IrMn thicknesses and all temperatures. In addition, our results indicate that H_E is smaller in nanodots at low measurement temperature due to the presence of disordered phases at the edges. Concerning H_C, our data show that it can be either larger or smaller in nanodots depending on the measurement temperature.

I. INTRODUCTION

The phenomenon of EB [1-4] has been extensively investigated in the last few decades, mainly in continuous films, from both experimental and fundamental points of view. EB occurs due to the coupling at the interface between ferromagnetic (F) and AF materials and depends on various parameters such as bulk and interfacial exchange couplings, bulk anisotropies, layer thicknesses, measurement and cooling temperatures ... Among these parameters, the measurement temperature and the AF layer thickness (t_{AF}) dependence of EB properties are the most frequently investigated from an experimental point of view. It should be noted that most of the theoretical models for EB properties do not account for thermal effects [5-9]. Recently, many experimental studies were conducted to well understand the thermal effects on the EB properties and they have shown some common behaviors of EB properties and some contradictory behaviors [10-17]. The main common behavior is that the exchange field H_E and the coercive field H_C decrease as the temperature increases at low temperatures. As the temperature increases, H_C increases and reaches a peak, while H_E still decreases in some studies [10-14] or increases and reaches a peak in other studies [15-17]. At higher temperatures, both H_E and H_C decrease again with increasing temperature. Now, considering the effect of t_{AF} the results indicate either a decrease [18,19] or a maximum [20, 21] of H_E as t_{AF} increases. The decrease of H_E is usually ascribed, in a random field model, to the presence of AF domains, whose structure strongly depends on t_{AF} [7,22, 23]. The presence of a maximum in H_E is attributed to a thermal effect on the stability of the grains.

More recently, since EB is used in spintronic devices such as spin valves and magnetic tunnel junctions [24, 25], and because of the necessity of increasing the magnetic storage density and reducing devices sizes [26], investigations have been carried out on nanodots with lateral sizes of few hundred nanometers [27]. Then, in addition to the various parameters which affect EB properties in continuous films, size and boundary effects play an important role in nanodots which complicates the understanding of EB properties. Indeed, contradictory results on H_E in nanodots compared to that of continuous films have been reported. For example, in NiFe/IrMn bilayers, it was observed that H_E at room temperature is larger in nanodots for thicknesses $t_{IrMn} > 11$ nm and smaller below this thickness compared to continuous films [18,28]. On the other hand, in Ref. [29] opposite results have been found. In another recent study on Co/IrMn nanodots at room temperature [20], it was shown that the dot lateral size has no significant effect on H_E ($3\ \text{nm} \leq t_{IrMn} \leq 15\ \text{nm}$). For the same system Co/IrMn ($t_{IrMn} = 7$ nm), it was observed that H_E at 4 K is smaller in nanodots than in

continuous films [30]. An important difference between nanodots and continuous films is the dot edges which consist of additional locations for the formation of disordered magnetic phases [30]. Nevertheless, few numerical studies on EB properties in F/AF nanodots have been carried out. A granular approach has shown a significant difference in H_E between nanodots and continuous films [31]. However, we wish to emphasize that the model used is rather simple since it does not include disordered phases neither at the F/AF interface, nor at the edges in the AF layer although these disordered phases have significant effect on EB properties [7,32,33]. Finally, let us mention an atomistic model which has shown an increase of H_E for systems patterned with small FM dots compared to continuous films [34].

In this study, we investigate EB properties of square F/AF nanodots and continuous films based on a granular model which accounts for the disordered interfacial phases by considering less stable magnetic grains at the interface in the AF layer [35, 36]. In addition, we model the effect of the nanofabrication process by the presence of less stable grains at the edges of the nanodots in the AF layer as experimentally demonstrated [30]. We first study the effect of the AF thickness on the EB properties of nanodots in comparison with continuous films at room temperature. Then we investigate the effect of temperature on the EB properties of nanodots and continuous films. In these two cases, our results are compared to experimental data on Co/IrMn bilayers. Our work is carried out by kinetic Monte Carlo simulations.

The remaining of the paper is organized as follows: The model and simulation technique are described in Sec. II. Numerical results of the effect of the AF thickness and temperature in Co/IrMn nanodots and continuous films in comparison with experimental data are given in Sec. III, and a conclusion is given in Sec. IV.

II. MODEL AND SIMULATION

The model is essentially that described in details in Refs [35, 36]. The F and AF layers are modeled by sets of grains coupled by exchange interactions. Since we assume columnar growth, they have the same granular microstructure which is created using a Voronoi tessellation [37] in two-dimensions. In nanodots, we model the effect of the nanofabrication process by the presence of grains with reduced areas at the edges due to grain cutting in the two layers. In Fig. 1 we present the top view of the granular microstructure for the continuous film and a nanodot, and the corresponding grain volume distribution for each case.

Importantly, the presence of smaller grains at the edges is noticeable in the nanodot compared to the continuous film.

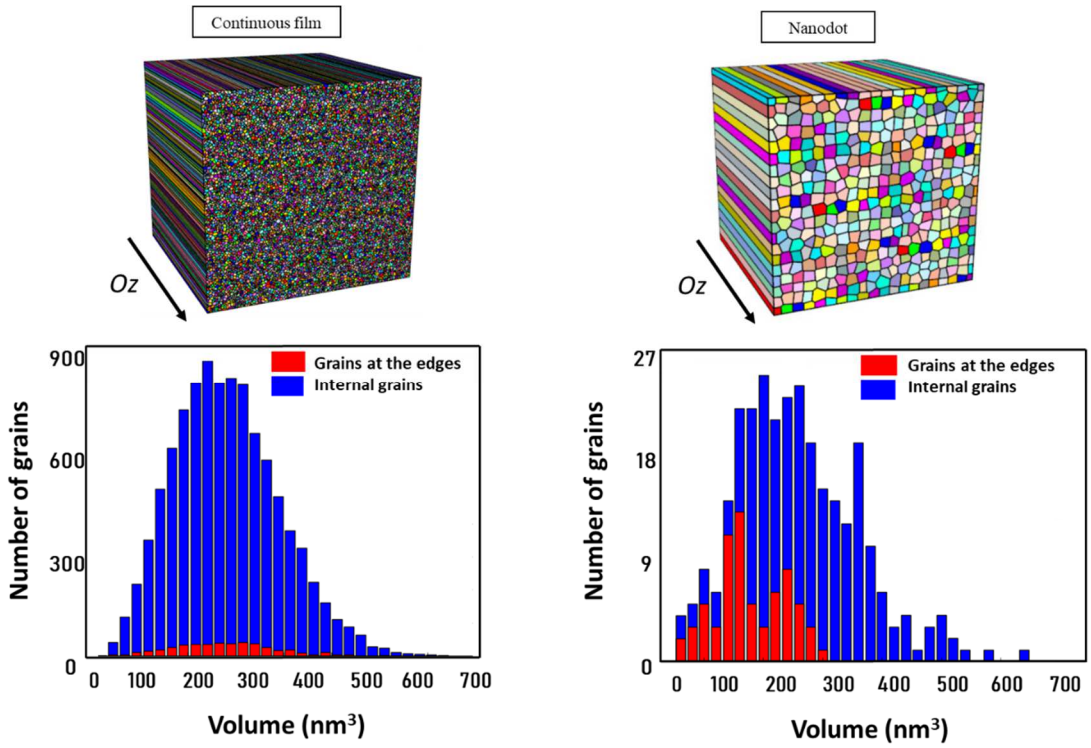

Fig. 1. (Color online) Top view of the granular microstructure created by Voronoi tessellation for the continuous film (10^4 grains) and a nanodot (289 grains), and the corresponding grains volume distribution.

In addition to F and AF grains, small grains (SG) of thickness $t_{SG} < t_{AF}$ are spread randomly over the F/AF interface within the AF layer in both nanodots and continuous films (Fig. 2) [35, 36]. These SG take into account disordered interfacial phases [7-32, 33] due to magnetic frustration produced by defects at the F/AF interface (e. g. interlayer diffusion and stacking faults). So, we consider that these SG exhibit altered magnetic properties (reduced anisotropy and coupling compared to the bulk AF grains). Assuming that the disordered interfacial magnetic phases extended over 3-4 atomic planes [38, 39], we set t_{SG}= 2 nm. Since, the fraction of SG at the F/AF interface x_{SG} may be varied between about 20% and 80%, as it depends on the fabrication process [40], we set x_{SG} to an average value of 50% in both nanodots and continuous films. In addition to that, we assume that the grains which are at the edges in the AF layer in nanodots (which will be referred as SG_E) exhibit the same magnetic

properties as the SG (Fig. 2) [30]. Accordingly, the fraction of grains with altered magnetic properties (SG and SG_E) is larger in nanodots since there is no SG_E in continuous films. Note that since $t_{SGE} = t_{AF}$ is larger than t_{SG}, the blocking temperature (T_B) distribution of a nanodot differs from that a continuous film.

The exchange energy between two grains is

$$E_{ex} = -J_{ij}\, \boldsymbol{\sigma}_i.\boldsymbol{\sigma}_j$$

where J_{ij} is the exchange constant ($J_{F\text{-}AF}$, $J_{F\text{-}SG}$ or $J_{F\text{-}F}$) and $\boldsymbol{\sigma}_i$, $\boldsymbol{\sigma}_j$ are unit vectors representing the magnetization orientation of a F grain, a SG, a SG_E or the interfacial uncompensated magnetization orientation of an AF grain. Note that the AF grains are not linked to each other [41,43], and nor are the SG and the SG_E (Fig. 2). Indeed the SG (and SG_E) and the AF grains are not linked to each other because such couplings do not affect directly the exchange bias properties of the bilayer. The couplings which contribute directly to H_E are the interfacial couplings: between the F grains and the AF grains ($J_{F\text{-}AF}$) and between the F grains and the smaller grains ($J_{F\text{-}SG}$) (the smaller grains are the SG in continuous films and the SG and SG_E in case of nanodots). Actually, a coupling between SG or SG_E or between AF grains would slightly affect their blocking temperature and thus could affect very slightly the exchange bias properties, so we have neglected them. In addition, concerning SG (or SG_E), couplings between them are expected to be small because of the non-collinearity of the spins in the disordered interfacial and edges phases, we expect that they do not affect the exchange bias properties. Assuming an uniaxial anisotropy energy along a common easy axis (y-axis) in the plane of the layer, the anisotropy energy is

$$E_a = -K_i\, V_i\, (\boldsymbol{\sigma}_i.\boldsymbol{e}_y)^2$$

where K_i is the anisotropy constant per unit volume (K_F, K_{AF} or K_{SG}) and V_i is the volume of the grain. We make this assumption for simplicity and also because we think that the results would not change qualitatively. Indeed, in case of random easy axes, the energy barriers to overcome during the reversal of the grains would be slightly modified which result in a small change in the blocking temperature of the grains. So, only a small change in our results could be observed. Finally, let us mention that such a magnetic texture could be obtained by applying an external field along the y-axis during the fabrication of the samples. A linear temperature dependence of the anisotropy constants per unit volume is implemented [44, 14] with $T_N = 690$ K [3]. Also, a Zeeman term

$$E_Z = -\mu_0 \boldsymbol{H}.\boldsymbol{m}_i$$

is taken into account where $\boldsymbol{m}_i$ is the magnetic moment of a F grain or a SG or a SG_E (in the nanodots) and **H** is the field applied along the *y*-axis. The magnetic moments m_i of F grains, SG and SG_E are calculated according to $m_i = M\,V_i$ where M is the magnetization of the grain and V_i is its volume. For the F grains, we have taken the Co magnetization $M = 1{,}44\times10^6$ A m^{-1} [45].

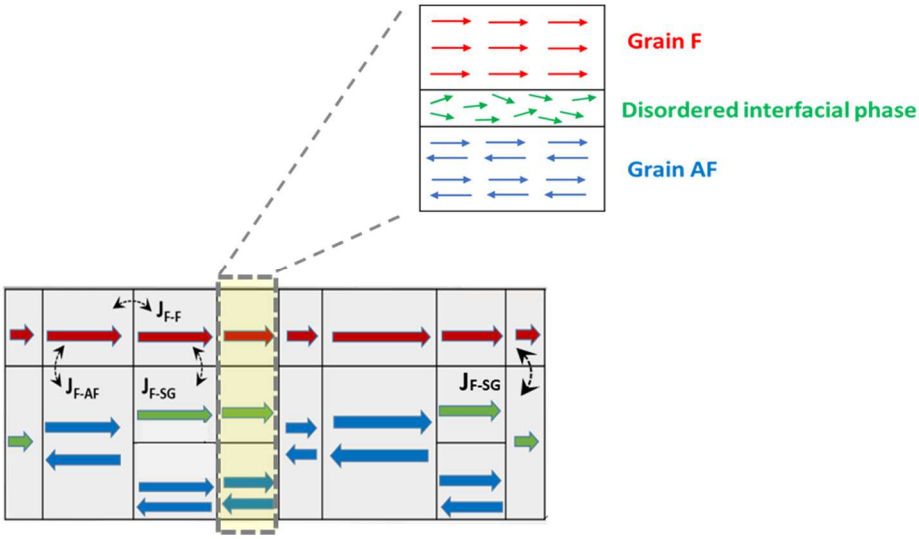

Fig. 2. (Color online) Sketch of the F/AF nanodot with SG randomly spread over the F/AF interface (in green) and SG_E at the edges in the AF layer (in green too). The small sketch above represents the collinear atomic moments of one F grain and one AF grain, and the non-collinear atomic moments of the disordered interfacial phase which are on-average along the *y*-axis as shown in the large sketch.

Some parameters of our model can be estimated from experimental results. For example, from experimental values of H_E [19], we found that $j_{F\text{-}AF} = 4.5\times10^{-4}$ J m^{-2} is a reasonable value in Co/IrMn bilayers. Likewise, the 0 K anisotropy constant for the AF grains was estimated to be $K_{AF}^0 = 4\times10^5$ J m^{-3} [46]. By contrast, the coupling per unit area, $j_{F\text{-}SG}$, and the effective anisotropy of SG and SG_E are unknown. However, $j_{F\text{-}SG}$ is assumed to be smaller than $j_{F\text{-}AF}$, so we set $j_{F\text{-}SG} = 3\times10^{-4}$ J m^{-2}. The effective anisotropy of the SG was also assumed to be weaker than that of the AF grains [30], we arbitrarily set K_{SG}^0 to $0.75\,K_{AF}^0$. In order to be in the weak coupling regime where the exchange field is independent on the F coupling ($j_{F\text{-}F}$) and there is

no variability between one nanodot to another, we choose $j_{F\text{-}F} = 10^{-4}$ J m^{-2} [47]. The fixed parameters of all our simulations are summarized in Table 1.

$j_{F\text{-}F} = 10^{-4}$ J m^{-2}	$j_{F\text{-}AF} = 4.5\times10^{-4}$ J/m^2	$j_{F\text{-}SG} = 3\times10^{-4}$ J/m^2
$T_N = 690$ K	$K_{AF}^0 = 4\times10^5$ J/m^3	$K_{SG}^0 = 3\times10^5$ J/m^3
$x_{SG} = 50\%$	$t_{SG} = 2$ nm	$t_{SGE} = t_{AF}$

Table 1. Fixed parameters of all our simulations.

Our Monte Carlo simulations [14,35,48,49] are capable of simulating cooling or heating under an external magnetic field. Thus, we can calculate the temperature dependence of the magnetic properties such as hysteresis loops from which the exchange and the coercive fields can be extracted.

III. RESULTS AND DISCUSSION

For all results presented below, we have simulated an initial field cooling (FC) from T_0 down to T_f. The hysteresis loops are simulated at a fixed $T_M = 298$ K in Sec. III.A or at increasing T_M ($T_f \leq T_M < T_0$) in Sec. III.B. To ease the understanding, we want to emphasize that the grains (in the AF layer) in contact with the F layer can be separated into three groups depending on their T_B and only one group contributes to H_E: (i) the grains with $T_B > T_0$, are not polarized by the external field and thus have a zero net magnetization and do not contribute to H_E; (ii) the grains with $T_M < T_B < T_0$, are polarized by the external field and are blocked at the measuring temperature T_M, so they contribute to H_E; (iii) the grains with $T_B < T_M$, are polarized by the external field but they are superparamagnetic at T_M so they do not contribute to H_E. Since, the experimental data that we compare with them correspond to an average over numerous nanodots, we therefore average our simulation results over several nanodots. We found that 60 nanodots of averaging is enough for convergence.

A. Effect of the AF thickness ($T_M = 298$ K)

In this part, we study the influence of the AF thickness on the EB properties, and then we compare our results with experimental data presented in Ref. [20]. To do so, we model Co/IrMn bilayers with $t_{Co} = 5$ nm and various t_{IrMn} (3 nm < t_{IrMn} < 14 nm). For each value of t_{IrMn}, the hysteresis loops are simulated at $T_M = 298$ K after FC under $H_{FC} = 2$ kOe from

$T_0 = 473$ K to $T_f = 298$ K. Figure 3 presents the hysteresis loops for $t_{IrMn} = 4$, 8 and 14 nm for the continuous film and nanodots. The t_{IrMn}-dependence of H_E in comparison with experimental data is shown in Fig. 4 [20]. Similar to the experimental data, our results show that the H_E curve exhibits a maximum in both cases of nanodots and continuous film. Note that these maxima are found at a slightly larger thickness than that reported experimentally (6.5 nm).

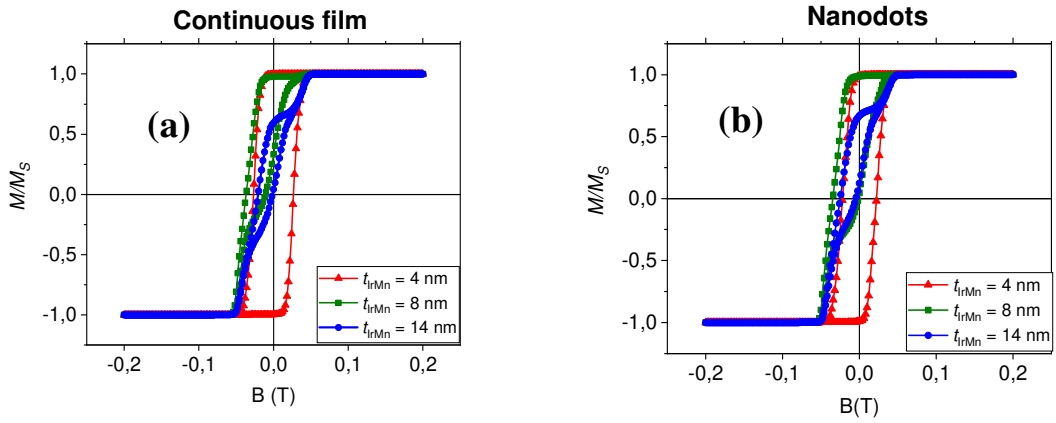

Fig. 3. (Color online) Simulated hysteresis loops at 298 K for various t_{IrMn}, for (a) the continuous film and (b) nanodots (averaged over 60 nanodots).

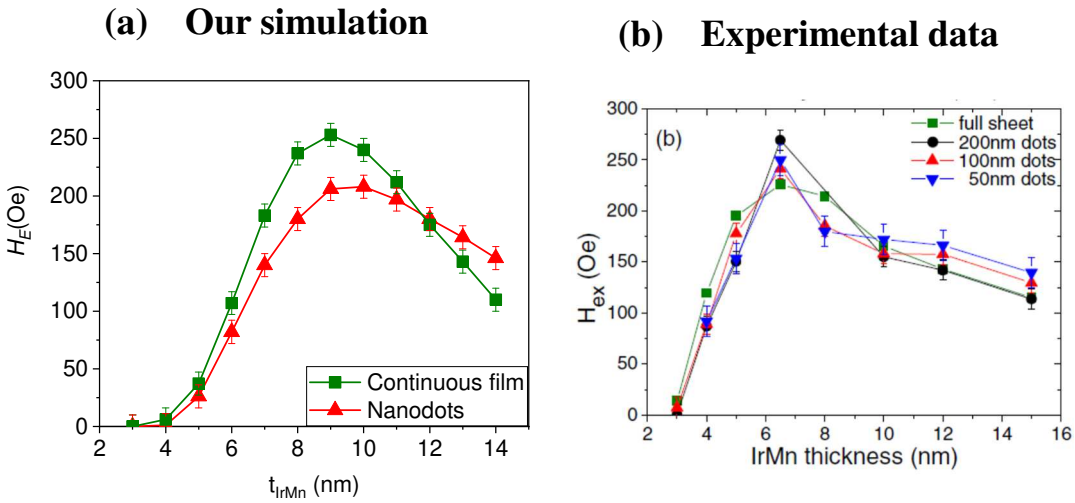

Fig. 4. (Color online) (a) Simulated t_{IrMn}-dependence of H_E measured at $T_M = 298$ K for Co/IrMn bilayers in comparison with (b) experimental data [20].

The behavior of H_E results from the t_{IrMn}-dependence of the fraction of grains in contact with the F layer which contribute to H_E, namely those which have blocking temperatures between T_M =298 K and $T_0 = 473$ K. More precisely, in the continuous film, SG do not contribute to

H_E since their T_B are smaller than 298 K (Fig. 5), while only a fraction of AF grains does contribute where this fraction depends on t_{IrMn}. For small thicknesses (Fig. 5.a), the fraction of AF grains which contributes to H_E is small and thus the value of H_E is small. When t_{IrMn} increases, this fraction increases and reaches a maximum at $t_{IrMn} \approx 9$ nm (Fig. 5.b) leading to a maximum in H_E. For $t_{IrMn} > 9$ nm, the fraction of the contributing AF grains decreases and thus H_E (Fig. 5.c). The small shift of our curves toward higher thicknesses compared to the experimental data is due to the small shift of the blocking temperature distribution of the AF grains in our model compared to the experimental one. Note that no difference between nanodots and the continuous films can be detected in experimental data due to error bars whereas our results indicate a smaller H_E in nanodots for $t_{IrMn} < 12$ nm, and a larger one if $t_{IrMn} > 12$ nm. This can be explained by the contribution of SG_E in nanodots which becomes more pronounced as t_{IrMn} increases. For $t_{IrMn} < 12$ nm, all SG_E are superparamagnetic and do not contribute to H_E, therefore the simulated values of H_E are slightly smaller than that in continuous films. However, for $t_{IrMn} > 12$ nm, most of SG_E contribute to H_E, and thus the simulated values of H_E are slightly larger than that in continuous films.

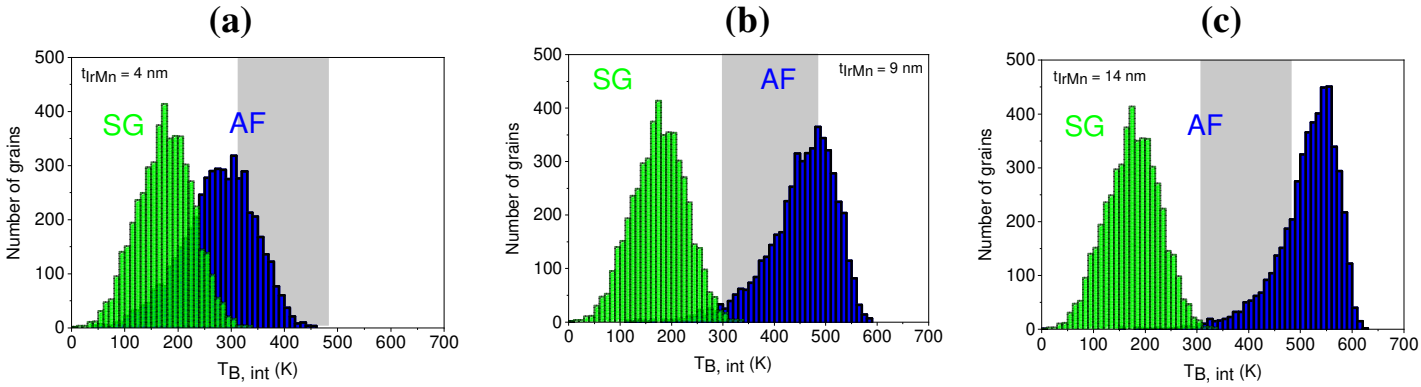

Fig. 5. (Color online) Intrinsic blocking temperature distributions for the grains in contact with the F layer at the interface in a Co/IrMn continuous film for (a) $t_{IrMn} = 4$ nm, (b) $t_{IrMn} = 9$ nm and (c) $t_{IrMn} = 14$ nm (the grey rectangles indicate the grains which contributes to H_E)

The t_{IrMn}-dependence of H_C is plotted in Fig. 6 in comparison with experimental data [20]. Our results reproduce qualitatively the experimental observations in a continuous film with a maximum of H_C at $t_{IrMn} = 3$-4 nm. In regards to H_C, the grains which contribute are those which are in contact with the F layer and having $T_B \approx T_M$. Since all SG have $T_B < T_M$ for all IrMn thicknesses (see Fig. 5), only a fraction of the AF grains in contact with the F layer contribute to H_c. Then according to Fig. 5, it can be seen that the fraction of these grains is

maximum at $t_{IrMn} = 4$ nm and decreases for $t_{IrMn} > 4$ nm which explains the behavior of H_C.

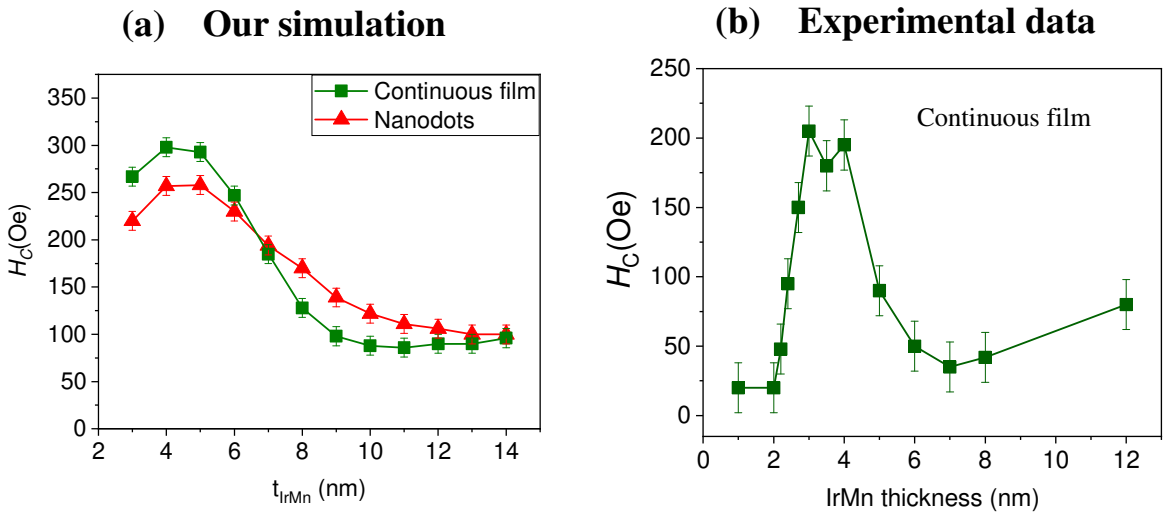

Fig. 6. (Color online) (a) Simulated t_{IrMn}-dependence of H_C measured at $T_M = 298$ K for Co/IrMn bilayers in comparison with (b) experimental data [20].

Comparing the case of the continuous film with nanodots, our results indicate that H_C is smaller in nanodots for $t_{IrMn} < 7$ nm while it is larger when $t_{IrMn} > 7$ nm. This is because the fraction of grains which contribute to H_C is smaller in nanodots for $t_{IrMn} < 7$ nm due to the presence of the SG_E which are superparamagnetic and thus do no contribute to H_C. However, for 7 nm $< t_{IrMn} <$ 12 nm, H_C is larger in nanodots because, the blocking temperatures of SG_E becomes closer to T_M, so they contribute to H_C.

B. Effect of the temperature and AF thickness

In this section, we study the effects of the AF thickness on the temperature dependence of the exchange and coercive fields in comparison with experimental data [19]. For that we consider a Co/IrMn bilayer with $t_{Co} = 4$ nm and various IrMn layer thicknesses ($t_{IrMn} = 3$ nm, 9 nm and 15 nm). The simulated procedure consists of a FC under $H_{FC} = 4$ kOe from $T_0 = 550$ K down to $T_f = 2$ K. Then successive hysteresis loops are simulated at increasing temperatures $T_M \geq 2$ K. The simulated temperature dependence of H_E and H_c for various t_{IrMn} in the continuous film is shown in Fig. 7 in comparison with those of Ref. [19].

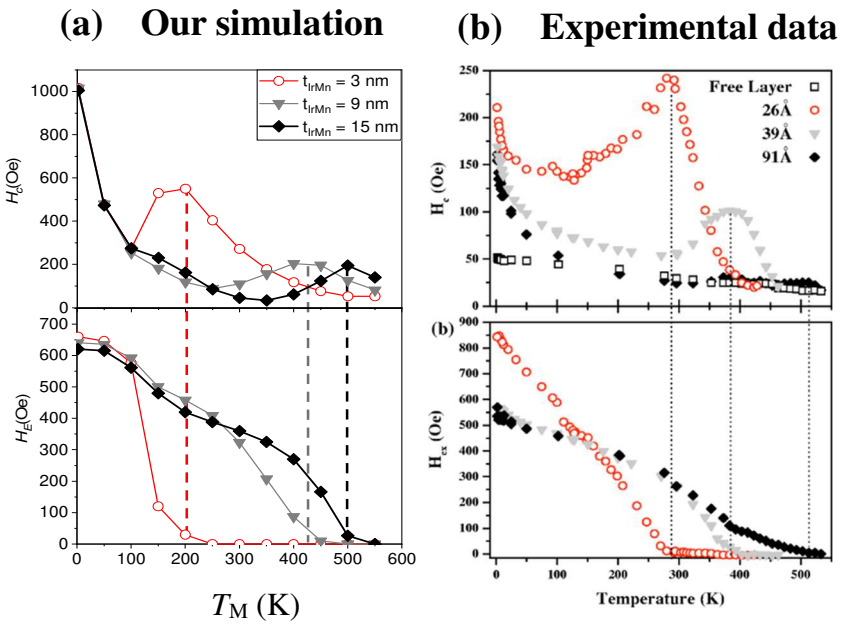

Fig. 7. (Color online) (a) Simulated temperature dependence of H_E and H_c in Co/IrMn bilayers (for various t_{IrMn} =3 nm, 9 nm and 15 nm) in the continuous film in comparison with (b) experimental data [19].

Concerning H_E, a good qualitative agreement with experimental data is obtained above 100 K: H_E decreases as T_M increases and vanishes at a temperature which increases with t_{IrMn}. The decrease of H_E is due to the increase of the fraction of superparamagnetic grains in contact with the F layer (AF grains and SG) when T_M increases. Note that the decrease below 200 K is attributed to the SG, *i.e.* to the disordered interfacial phases since a model without SG cannot reproduce this decrease [14]. Then H_E vanishes at a temperature corresponding to the maximum blocking temperature of the AF grains which increases with $V_{AF}^{max} \propto t_{IrMn}$. We can compare the vanishing temperature of H_E with the maximum of the intrinsic blocking temperature $T_B^{max} = \frac{K_{AF}^0 V_{AF}^{max} T_N}{k_B T_N \ln(2n) + K_{AF}^0 V_{AF}^{max}}$ where n is the number of Monte Carlo steps [36] (Fig. 8). The vanishing temperature of H_E exhibits, as expected, the same t_{IrMn}-dependence as T_B^{max}, however it is roughly 150-200 K lower than T_B^{max} clearly showing that the coupling with

the neighboring F grains results in a decrease of the (effective) blocking temperature of the AF grains. Finally, note that, at $T_M = 2$ K, the simulated value of H_E slightly decreases as t_{IrMn} increases. This is because the fraction of grains which contribute to H_E (those with $T_B < 550$ K) decreases as t_{IrMn} increases as shown in Fig. 9.

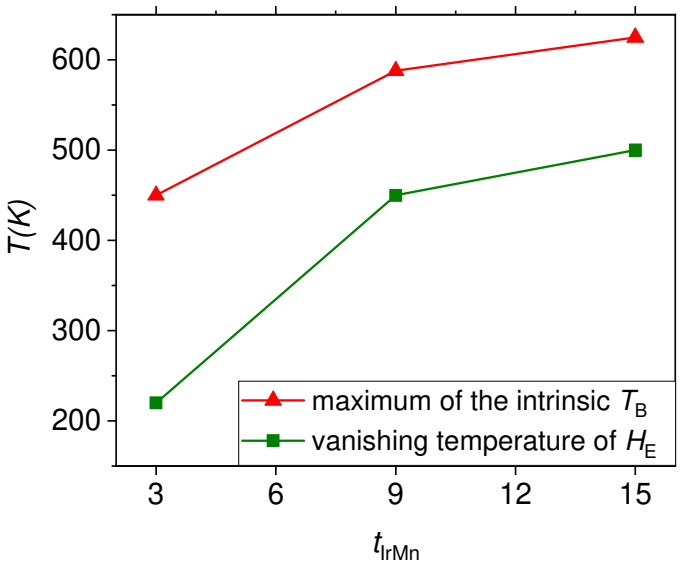

Fig. 8. Comparison between the vanishing temperature of the simulated H_E and the maximum of the intrinsic blocking temperature versus t_{IrMn}.

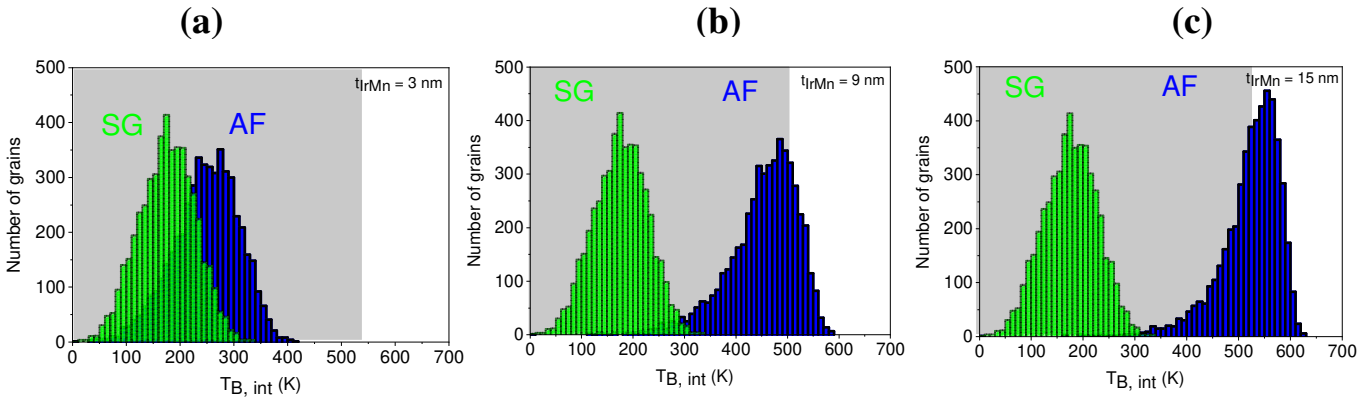

Fig. 9. (Color online) Intrinsic blocking temperature distributions for the grains in contact with the F layer at the interface in a Co/IrMn continuous film for (a) $t_{IrMn} = 3$ nm, (b) $t_{IrMn} = 9$ nm and (c) $t_{IrMn} = 15$ nm (the grey rectangles indicate the grains which contribute to H_E at $T_M = 2$ K).

Regarding H_C, a good qualitative agreement with experimental data is also obtained. In particular, a maximum in H_C is observed simultaneously at the vanishing temperature of H_E. This maximum shifts toward higher temperatures and its amplitude decreases as t_{IrMn} increases. Actually, this maximum results from both the shift of the blocking temperature

distribution of AF grains as t_{IrMn} increases and the fact that only the AF grains having T_B close to T_M contributes to H_C (see Fig. 9).

In order to see the effects of reducing the lateral size, we perform the same simulations for nanodots with $t_{IrMn} = 9$ nm. The temperature dependence of H_E and H_C is plotted in Fig. 10 in comparison with that of a continuous film. The same behavior is observed in nanodots as in the continuous film. Note that at $T_M = 2$ K, all grains in contact with the F layer contribute to H_E, where H_E is smaller in nanodots due to the presence of SG_E at the edges (which are less coupled with the F layer than the AF grains). Note also that the location of the minimum and the maximum of H_c is shifted towards lower temperatures in nanodots. This is because the fraction of grains contributing to H_c, at low temperatures, increases in the nanodots due to presence of SG_E (Fig. 11).

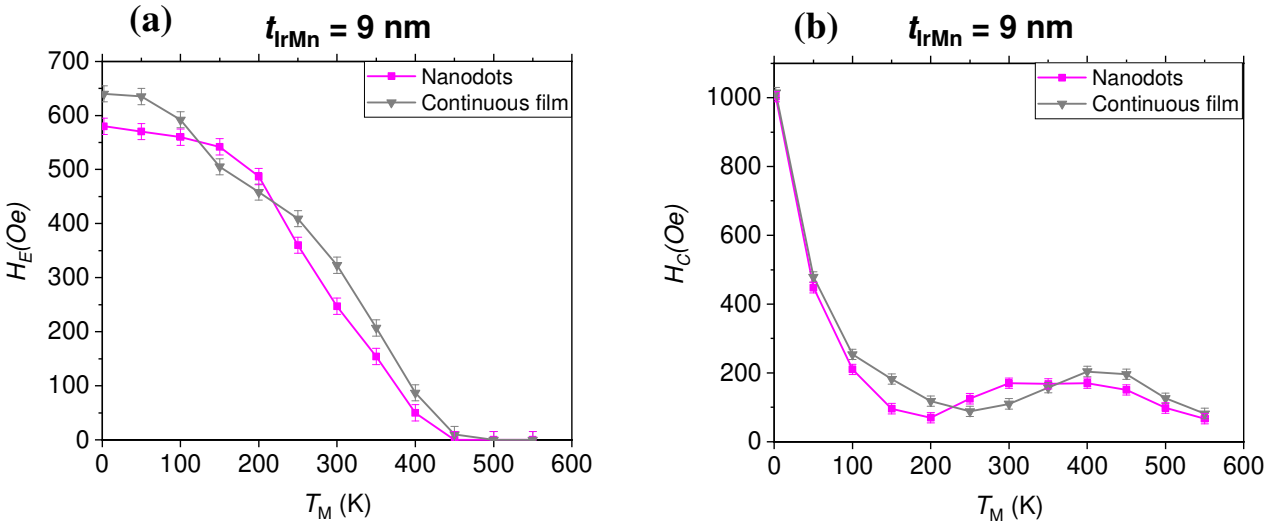

Fig. 10. (Color online) Simulated temperature dependence of (a) H_E and (b) H_C in Co/IrMn bilayers (t_{IrMn} =9 nm) in both nanodots and continuous film.

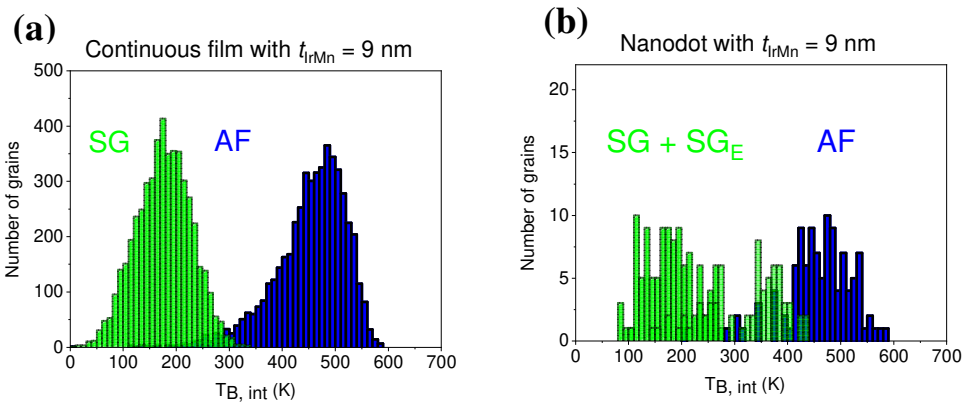

Fig. 11. (Color online) Intrinsic blocking temperature distributions of the grains in contact

with the F layer at the interface in a Co (4 nm)/IrMn (9 nm) for (a) the continuous film and (b) a nanodot.

IV. CONCLUSION

By using a granular model which takes into account disordered magnetic phases at the F/AF interface and at the edges in the AF layer in nanodots, we have proposed a comprehensive description of the AF thickness and temperature effects on the EB properties in Co/IrMn nanodots and in continuous films. Our model is based on the assumption of single domain grains and the disordered interfacial phases are modeled by less stable magnetic grains. Our numerical results are in good qualitative agreement with experiments for various AF thicknesses and measurement temperatures. More precisely, the AF thickness dependence of H_E exhibits a maximum at room temperature. Also, the temperature dependence of H_E shows a decreases at low temperatures due to the disordered phases and vanishes at the maximum blocking temperature of the AF grains for which H_C is maximum. Our results show that the simulated values of H_E in nanodots can be smaller or larger than that in continuous films depending on the AF thickness and the measurement temperature due to contribution of the disordered phases at the edges in the AF layer. Note that these results provide an explanation of the various experimental results found in literature about the comparison between EB properties of nanodots and continuous films. To achieve a deeper understanding of the disordered interfacial phases, it would be of great interest to use an atomic approach which takes into account grain boundaries and atomic interdiffusion in the AF layer. Note that to avoid huge computational time, such a study would be restricted to nanodots.

Acknowledgments

This project is funded by the Région Normandie and the European Union. Europe invests in Normandy with the European Regional Developement Fund (ERDF) – MAGMA project. The authors acknowledge the Centre Régional Informatique et d'Applications Numériques de Normandie (CRIANN) where simulations were performed as Project No. 2010006. We also thank Ahmed Albaalbaky for critical reading of the manuscript.

References

[1] W. H.Meiklejohn and C. P. Bean, Phys. Rev. **102**, 1413 (1956).

[2] W. H. Meiklejohn and C. P. Bean, Phys. Rev. **105**, 904 (1957).

[3] J. Noguès and I. K. Schuller, J. Magn. Magn. Mater. **192**, 203 (1999).

[4] A. E. Berkowitz and K. Takano, J. Magn. Magn. Mater. **200**, 552 (1999).

[5] W. H. Meiklejohn, J. Appl. Phys. **33,** 1328 (1962).

[6] D. Mauri, H. C. Siegmann, P. S. Bagus and E. Kay, J. Appl. Phys. **62**, 3047 (1987).

[7] A. P. Malozemoff, Phys. Rev. B. **35,** 3679 (1987).

[8] L. Néel, Ann. Phys. **2**, 61 (1967).

[9] K. Takano, R. H. Kodama, A. E. Berkowitz, W. Cao and G. Thomas, Phys. Rev. Lett. **79**, 1130 (1997).

[10] W. Pan, N.-Y. Jih, C.-C. Kuo, and M.-T. Lin, Appl. Phys. Lett. **95**, 7297 (2004).

[11] J. P. Nozières, S. Jaren, Y. B. Zhang, A. Zeltser, K. Pentek, and V. S. Speriosu, J. Appl. Phys. **87**, 3920 (2000).

[12] J. Richy, T. Hauguel, J.-Ph. Jay, S. P. Pogossian, B. Warot-Fonrose, C. J. Sheppard, J. L. Snyman, A. M. Strydom, J. Ben. Youssef, A. R. E. Prinsloo, D. Spenato, and D. T. Dekadjevi, J. Phys. D:Appl. Phys, **51**, 12, (2018).

[13] R. A. Khan, H. T. Nembach, M. Ali, J. M. Shaw, C. H. Marrows, and T. A. Moore, Phys. Rev. B **98**, 064413 (2018).

[14] D. Ledue, A. Maitre, F. Barbe and L. Lechevallier, J. Magn. Magn. Mater, **372,** 134, (2014).

[15] M. Dunz, J. Schmalhorst, and M. Meinert, AIP ADVANCES, **8**, 056304 (2018).

[16] C. Hou, H. Fujiwara, K. Zhang, A. Tanaka and Y. Shimizu, Phys. Rev. B. **63**, 024411 (2000).

[17] J.-G. Hu, G. Jin, A. Hu and Y.-Q Ma, Eur. Phys. J. B **40**, 265 (2004).

[18] V. Baltz, J. Sort, S. Landis, B. Rodmacq and B. Dieny, Phys. Rev. Lett. **94**, 117201 (2005).

[19] M. Ali, C. H. Marrows, M. Al-Jawad and B. J. Hickey, Phys. Rev. B **68**, 214420 (2003).

[20] G. Vinai, G. Gaudin, J. Moritz, J. Vogel, I. L. Prejbeanu and B. Dieny, J. Phys. D:Appl. Phys. **47**, 195302 (2014).

[21] G. Vallejo-Fernandez, L. E. Fernandez-Outon and K. O'Grady J. Phys. D:Appl. Phys. **41**, 112001 (2008).

[22] A. Misra, U. Nowak and K. D. Usadel, J. Appl. Phys. **95**, 1357 (2004).

[23] U. Nowak, K.D. Usadel, J. Keller, P. Miltény, B. Beschoten and G. Guntherodt, PRB **66**, 014430 (2002).

[24] I. L. Prejbeanu, M. Kerekes, R. C. Sousa, H. Sibuet, O. Redon, B. Dieny and J. P. Nozieres, J. Phys. Cond. Matt. **19**, 165218 (2007).

[25] V. Baltz, A. Manchon, M. Tsoi, T. Moriyama, T. Ono and Y. Tserkovnyak, Rev. Mod. Phys. **90**, 015005 (2018).

[26] C. Chappert, A. Fert and F. N. Van Dau, Nat. Mater. **6**, 813 (2007).

[27] J. Noguès J. Sort, V. Langlais, V. Skumryev, S. Surinach, J. S. Munoz, M. D. Baro and I. K. Schuller, Physics Reports **422**, 65 (2005).

[28] V. Baltz, J. Sort, B. Rodmacq, B. Dieny and S. Landis, Phys. Rev. B **72**, 104419 (2005).

[29] Y. Shen, Y. Wu, H. Xie, K. Li, J. Qiu, and Z. Guo, J. Appl. Phys. **91**, 8001 (2002).

[30] V. Baltz, G. Gaudin, P. Somani and B. Dieny, Appl. Phys. Lett. **96**, 262505 (2010).

[31] G. Vallejo-Fernandez and J. N. Chapmam, Appl. Phys. Lett. **94**, 262508 (2009).

[32] M. P. Proenca, J. Ventura, C. T. Sousa, M. Vazquez and J. P. Araujo, Phys. Rev. B **87**, 134404 (2013).

[33] F. Spizzo, E. Bonfiglioli, M. Tamisari, A. Gerardino, G. Barucca, A. Notargiacomo, F.

Chinni and L. Del Bianco, Phys. Rev. B **91**, 064410 (2015).

[34] G. Garcia , M. Kiwi, J. Mejia-Lopez and R. Ramirez, J. Magn. Magn. Mater. **322**, 3329 (2010).

[35] G. Lhoutellier, D. Ledue, R. Patte, F. Barbe, B. Dieny and V. Baltz, J. Phys. D: Appl.Phys. **48,** 115001 (2015).

[36] G. Lhoutellier, D. Ledue, R. Patte and V. Baltz, J. Appl. Phys. **120**, 193902 (2016).

[37] R. Quey, P. R. Dawson and F. Barbe, Comput. Methods Appl. Mech. Eng. **200**, 1729 (2011).

[38] L. Lechevallier, A. Zarefy, R. Lardé, H. Chiron, J.-M. Le Breton, V. Baltz, B. Rodmacq and B. Dieny, Phys. Rev. B **79**, 174434 (2009).

[39] L. Lechevallier, A. Zarefy, F. Letellier, R. Lardé, D. Blavette, J. M. Le Breton, V. Baltz, B. Rodmacq and B. Dieny, J. Appl. Phys. **112**, 043904 (2012).

[40] K. Akmaldinov, S. Auret, I. Dieny, and V. Baltz Appl. Phys. Lett. **103**, 042415 (2013).

[41] E. Fulcomer and S. H. Charap, J. Appl. Phys. **43**, 4190 (1972).

[42] D. Choo, R.W. Chantrell, R. Lamberton, A. Johnston and K. O'Grady, J. Appl. Phys. **101**, 09E521 (2007).

[43] B. Craig, R. Lamberton, A. Johnston, U. Nowak, R. W. Chantrell and K. O'Grady, J. Appl. Phys. **103**, 07C102 (2008).

[44] M. D. Stiles and R. D. McMichael, Phys. Rev. B **60**, 950 (1999).

[45] J. M. D. Coey, Magnetism and Magnetic Materials (Cambridge University Press, 2010).

[46] G. Vallejo-Fernandez, L. E. Fernandez-Outon and K. O'Grady, Appl. Phys. Lett. **91**, 212503 (2007).

[47] H. Kanso, R. Patte, V. Baltz and D. Ledue, Phys. Rev. B **99**, 054410 (2019).

[48] D. W. Heermann, Comput. Simul. Methods Theor. Phys. (Springer, Berlin) 2nd Ed. (1990).

[49] K. Binder and D. W. Heermann, Monte Carlo Simul. Stat. Phys. (Springer, Berlin) 2nd Ed. (1990).